Impact of lithiated cobalt oxide and phosphate nanoparticles on rainbow trout gill epithelial cells

Eric S. Melby, ^{a,d} Yi Cui, ^a Jaya Borgatta, ^b Arielle C. Mensch, ^a Mimi N. Hang, ^b William B. Chrisler, ^c Alice Dohnalkova, ^a John M. Van Gilder, ^{b,e} Catherine M. Alvarez, ^b Jordan N. Smith, ^c Robert J. Hamers, ^{b,} Galya Orr, ^{a,*}

* Corresponding Author: Galya Orr, Pacific Northwest National Laboratory, P.O.Box 999 MSIN K8-88, Richland, WA 99352 USA. Tel: 509-371-6127. galya.orr@pnnl.gov

^a Environmental Molecular Sciences Laboratory, Pacific Northwest National Laboratory, Richland, WA 99354

^b University of Wisconsin-Madison, Department of Chemistry, 1101 University Ave., Madison, WI, 53706

^c Biological Sciences Division, Pacific Northwest National Laboratory, Richland, WA 99354

^d Present address: Columbia Basin College, 2600 N 20th Ave., Pasco, WA 99301

^e Present address: Convergent Science, 6400 Enterprise Ln, Madison, WI 53719

KEYWORDS: Nanotoxicology, nanoparticle dissolution, lithium intercalation compound, oxidative stress, cathode material

ABSTRACT: Metal oxide and phosphate nanoparticles (NPs) are ubiquitous in emerging applications, ranging from energy storage to catalysis. Cobalt-containing NPs are particularly important, where their widespread use raises questions about the relationship between composition, structure, and potential for environmental impacts. To address this gap, we investigated the effects of lithiated metal oxide and phosphate NPs on rainbow trout gill epithelial cells, a model for environmental exposure. Lithium cobalt oxide (LCO) NPs significantly reduced cell viability at 10 µg/mL, while a 10-fold higher concentration of lithiated cobalt hydroxyphosphate (LCP) NPs was required to significantly reduce viability. Exposure to Li⁺ and Co²⁺ alone, at concentrations relevant to ion released from the NPs, did not reduce cell viability and minimally impacted reactive oxygen species (ROS) levels. Both LCO- and LCP-NPs were found within membrane-bound organelles. However, only LCP-NPs underwent rapid and complete dissolution in artificial lysosomal fluid. Unlike LCP-NPs, LCO-NPs significantly increased intracellular ROS, could be found within abnormal multilamellar bodies, and induced formation of intracellular vacuoles. Increased p53 gene expression, measured in individual cells, was observed at sub-toxic concentrations of both LCO- and LCP-NPs, implicating both in inductions of cellular damage and stress at concentrations approaching predicted environmental levels. Our results implicate the intact NP, not the dissolved ions, in the observed adverse effects and show that LCO-NPs significantly impact cell viability accompanied by increase in intracellular ROS and formation of organelles indicative of cell stress, while LCP-NPs have minimal adverse effects, possibly due to their rapid dissolution in acidic organelles.

INTRODUCTION

Nanostructured cobalt oxides and cobalt phosphates find ubiquitous applications ranging from energy storage to catalysis. The sheet-like lithium intercalation compound, lithium cobalt oxide (LCO), is the most commonly used cathode material for lithium-ion batteries(Nitta et al. 2015; Goodenough & Park 2013) and is also an attractive catalyst for electrochemical water oxidation.(Wang et al. 2017; Wu et al. 2017; Lu et al. 2014) While LCO is used as sintered aggregates of nanoparticles (NPs) with primary particle diameter on the order of 100 nm, under operating conditions these particles fracture into smaller, sheet-like "nano-flakes".(Wang et al. 1999) In addition, there is interest in decreasing the size of cathode materials in an effort to improve battery performance through faster ion and electron transport and increased mechanical stability.(Poizot et al. 2000; Bruce et al. 2008; Nitta et al. 2015) Because LCO has relatively high reactivity and a propensity to dissolve in both aqueous (catalytic) and non-aqueous (energy storage) applications, (Wang et al. 2007; Lee et al. 2007) olivine-structured metal phosphate nanomaterials (metal = Fe, Mn, Ni, or Co) have emerged as potential alternatives due to their high thermal stability, cycling life, and attractive power properties. (Zaghib et al. 2013; Zaghib et al. 2011) Use of battery cathode materials has been guided by performance, cost, and operating safety, but the rapid expansion of Li-ion batteries and emerging catalysts increases the likelihood for their release into the environment during manufacture, use, or disposal. (Kang et al. 2013) Coupled with minimal infrastructure for recycling Li-ion batteries, (Dunn et al. 2015) it is critical that we understand the behavior and possible implications of lithiated metal oxide and phosphate NPs in the environment.

Despite a wealth of nanotoxicology studies, the impact of lithiated metal oxide and phosphate NPs on biological systems has received little attention. Exposing supported phospholipid bilayers to LCO-NPs induced phospholipid asymmetrization across the bilayer leaflets.(Dogangun et al. 2015) It has been observed that a reduction in *Shewanella oneidensis* MR-1 viability upon exposure to lithium nickel manganese cobalt oxide (NMC) NPs was the result of Ni and Co dissolution and toxicity.(Hang et al. 2016; Gunsolus et al. 2017) In *Daphnia magna*, acute studies showed LCO- and NMC-NPs had no effect at exposure concentrations up to 25 μ g/mL, but 21 day chronic exposures caused significant impacts on survival and reproduction at exposure concentrations $\leq 1 \mu$ g/mL.(Bozich et al. 2017) To further this work we have investigated the effect

of lithiated metal oxide and phosphate NPs on *Oncorhynchus mykiss* (rainbow trout) gill epithelial cells, a potential target for NP exposure in the aquatic environment. Previous studies have investigated the impact of tungsten carbide,(Kühnel et al. 2009) silica,(Vo et al. 2014) and silver(Yue et al. 2015; Yue et al. 2016) NP exposure on this cell type with a primary focus on the role of exposure media composition as assessed by viability assays.

Here we sought to expand the research beyond the effect of NP exposure on cell viability in an effort to begin to elucidate mechanisms underlying lithiated metal oxide and phosphate NP toxicity. Heavy metal dissolution from NPs has been shown to be either a complete or partial driver of NP toxicity, (Hang et al. 2016; Gunsolus et al. 2017; Xia et al. 2008; Kittler et al. 2010; Mihai et al. 2015) depending on the NPs and organisms being investigated. Using ICP-MS we quantified the dissolution dynamics of LCO and lithiated cobalt hydroxyphosphate (LCP) NPs in biological solutions as an initial attempt to decipher the impact of the intact NPs and the released ions on the gill epithelial cells. We further used transmission electron microscopy to investigate the cellular uptake of LCO- and LCP-NPs to determine if NPs may be subjected to acidic organelles that could enhance NP dissolution, ultimately resulting in an increase in the release of potentially toxic metal ions in the intracellular environment, as has been previously reported. (Mihai et al. 2015; Muller et al. 2010) In addition, we focused on intracellular effects of LCO- and LCP-NP exposure, including the generation of reactive oxygen species (ROS) and the regulation of cellular stress response. Finally, we determined the effect of these NPs on the regulation of p53 gene expression as an indicator of cellular stress response.(Liu & Kulesz-Martin 2001; Bartek & Lukas 2001; Ahamed et al. 2008) We utilized single molecule fluorescence in situ hybridization (smFISH) to quantify p53 mRNA copy number in individual cells,(Raj et al. 2008; Raj & Tyagi 2010) allowing the detection of subtle changes that might be buried or diluted otherwise in averaged cell population measurements.(Mitchell et al. 2016) While most studies focus on NP concentrations that lead to a detectable reduction in cell viability, quantifying p53 gene expression in individual cells allows investigations at a sub-toxic NP concentration to understand how environmentally relevant exposure concentrations(Sun et al. 2016) impact cellular functions. These results will contribute to the design of a framework that considers the potential environmental implications of lithiated metal oxide and phosphate NPs equally with their cost and performance when they are considered for use in technological applications.

MATERIALS AND METHODS

Synthesis of lithiated metal oxide and phosphate NPs. Lithium cobalt oxide (LCO) nanoparticles(Qian et al. 2012) were synthesized as previously reported. The synthesis protocol for lithiated cobalt hydroxyphosphate (LCP) nanoparticles was adapted from patent No. US 8,313,863,(Exnar & Drezen 2012).

Nanoparticle characterization. *TEM*. NPs freshly sonicated in water were immediately drop cast onto TEM grids prior to imaging with a Tecnai T-12 TEM (FEI) with a LaB₆ filament operating at 120 kV. Images were collected digitally using an Ultrascan 1000 CCD (Gatan).

XPS. NP samples were analyzed using a custom built ultra-high vacuum PHI system consisting of a monochromatic Al K α source and a hemispherical electron energy analyzer. The collected spectra were processed and analyzed using CasaXPS software.

XRD. All XRD characterization was performed on a Bruker d8 Advance powder diffractometer, using a copper Kα source and a 6 mm slit width. The X-ray patterns were matched to literature patterns using Bruker DIFFRAC.EVA and Crystal Diffract software.

Cell culture. Oncorhynchus mykiss (rainbow trout) gill epithelial cells (RTgill-W1, CRL-2523), Leibovitz's L-15 media (30-2008), and fetal bovine serum (FBS, 30-2021) were purchased from ATCC. Cells were grown in polystyrene culture flasks in Leibovitz's L-15 media supplemented with 10% FBS (referred to as 'media' throughout). Cells were incubated at 19°C in ambient atmosphere. Culture medium was replaced twice weekly, and cells were harvested for experiments and passage upon reaching 100% confluency. Adherent cells were removed by removing culture media, rinsing with 0.25% Trypsin-0.53 mM EDTA solution, and adding fresh Trypsin-EDTA solution until cells were detached (~10 minutes). Cells used in these experiments were between passages 3-20.

Nanoparticle preparation for exposure. LCO- and LCP-NPs were massed in a Labconco XPert Nano Enclosure, and a 1000 μ g/mL stock solution was made by adding culture medium. Nanoparticle solutions were sonicated in ice water using a Branson Digital Sonifier 450 operated at 300 W for 4 x 2.5 minutes. Fresh ice was added between each sonication step. Freshly sonicated nanoparticles were immediately diluted to the working concentration and used for gill cell exposures. The same procedure was used for unexposed control cells and cells exposed to Co²⁺

and Li⁺ (from CoCl₂ and LiCl, respectively) in the absence of NPs to control for sonication induced reactive oxygen species generation and protein denaturation. (Cohen et al. 2013)

Cell viability. Cell viability was determined using the CellTiter 96 AQ_{ueous} One Solution Cell Proliferation Assay (MTS) (G3580, Promega). Gill cells were seeded in 96 well plates at 5×10^4 cells per well in a total volume of 100 μ L. When cells reached 100% confluency, medium was removed and cells were exposed to 100 μ L of freshly prepared solutions of LCO- or LCP-NPs. For negative controls, Promega cell lysis solution was added 45 min before the end of the NP exposure period. After the NP exposure period cells were washed three times with 100 μ L media (to remove any unbound nanoparticles), incubated with 20 μ L MTS solution in 100 μ L media for 4 h at 19°C in ambient atmosphere, and the absorbance at 490 nm was determined using a Beckman Coulter DTX 880 Multimode Detector.

Transmission electron microscopy of trout gill epithelial cells. Transmission electron microscopy (TEM) was used to determine whether gill cells internalize LCO- and LCP-NPs following a 24 h exposure to 10 μg/mL NPs. Cells were embedded, sectioned to 70 nm sections, and imaged using a Tecnai T-12 TEM (FEI) with a LaB₆ filament operating at 120 kV. Images were collected digitally using an Ultrascan 1000 CCD (Gatan).

LCO- and LCP-NP dissolution in media and artificial lysosomal fluid: Nanoparticle stock solutions were prepared as described above to determine NP dissolution in media. To determine NP dissolution in artificial lysosomal fluid (ALF, pH 4.5),(Hedberg et al. 2012) NP stock solutions were prepared in phosphate buffered saline. Stock solutions were then diluted to $100 \mu g/mL$ in either media or ALF, and $1800 \mu L$ of NP solution was added to 35μ mm Petri dishes for 0, 1, 3, 6, 24, 35 and 35μ metri dishes for 35μ metri dishes for 35μ metri dishes for 35μ metri dishes, added to 35μ metrifuge tubes, and centrifuged 35μ min at 35μ metrical results filter devices, and the samples were centrifuged 35μ min at 35μ metrical results filter devices were used for more rapid sample preparation). Solution passing through the filter was collected for analysis. Dissolved lithium and cobalt concentrations were quantified using inductively coupled plasma mass spectrometry (ICP-MS).

Fluorescence imaging of intracellular ROS: Gill cells were seeded in 35 mm No. 1.5 glass bottom Petri dishes and cultured until reaching confluency prior to NP exposure. Following the NP exposure period, cells were rinsed three time with Live Cell Imaging Solution and incubated for 30 min with 10 μ M of the general oxidative stress indicator CM-H₂DCFDA (C6827, ThermoFisher Scientific) and 2.5 μ g/mL Hoechst 33342 (ThermoFisher Scientific) in Live Cell Imaging Solution. Following the incubation period cells were rinsed three times with Live Cell Imaging Solution and immediately imaged using a Zeiss LSM 710 confocal microscope with a 63x objective and 488 nm laser.

Flow cytometry to quantify intracellular ROS: Trout gill epithelial cells were seeded in 60 mm plasma-treated polystyrene Petri dishes and cultured until reaching confluency prior to NP exposure. Following the NP exposure period, cells were rinsed three time with Live Cell Imaging Solution and incubated for 30 min with 10 μM of the general oxidative stress indicator CM-H₂DCFDA (C6827, ThermoFisher Scientific) and 2.5 μg/mL Hoechst 33342 (ThermoFisher Scientific) in Live Cell Imaging Solution. Following the incubation period cells were rinsed three times with phosphate buffered saline and removed from the dish surface by a 10 min exposure to trypsin-EDTA solution (30-2101, ATCC). Cells were pelleted by centrifugation at 125 rcf for nine minutes, supernatant was removed, and cells were resuspended in complete medium for flow cytometry analysis.

Single molecule FISH for p53 gene expression: Single-molecule fluorescence in situ hybridization (smFISH) was used to quantify p53 gene expression at the single-cell level. 12 probes targeting p53 mRNA were designed and labeled with Alexa-647 (Integrated DNA Technologies, Inc.). The sequence information of all probes is provided in **Table S1**. Gill cells were seeded into No. 1.5 glass bottom dishes and cultured to reach 70-80% confluence when subjected to different treatments. The hybridization and imaging experiments followed the general protocol as established previously.(Raj et al. 2008; Raj & Tyagi 2010).

RESULTS

Characterization of lithium cobalt oxide (LCO) and lithiated cobalt hydroxyphosphate (LCP) NPs

Both LCO- and LCP-NPs exhibit a sheet-like morphology (Figure 1). LCO-NPs exhibit a platelike shape and smaller diameter (30-50 nm, in agreement with previous reports(Dogangun et al. 2015)), whereas the LCP-NPs regularly exhibit a more rectangular shape with sheet dimensions ranging from approximately 100-500 nm. Since NP exposures were conducted with NPs suspended in Leibovitz's L-15 growth medium, we utilized dynamic light scattering and electrophoretic light scattering to determine the apparent NP hydrodynamic diameter (d_h) and ζ potential, respectively, of particles suspended in growth medium. We refer to the dynamic light scattering results as "apparent d_h " and "apparent ζ potential" as the models used to determine these values assume a spherical particle. Apparent d_h values were in agreement with TEM images of the NPs suspended in water (LCO-NPs: 167 ± 30 nm; LCP-NPs: 475 ± 43 nm), and the apparent ζ potential values for both NPs were near neutral (LCO-NPs: -8.3 ± 4.5 mV; LCP-NPs: -0.4 ± 8.3 mV). Previous reports of X-ray photoelectron spectroscopy (XPS) analysis of the LCO-NPs confirmed the presence of the expected Li and Co peaks. (Dogangun et al. 2015) Our XPS analysis of the LCP-NPs identified the expected peaks for Li, Co, P, and O, as well as small amounts of N and C (a common surface contaminant) (Figure S1). We also characterized the LCO- and LCP-NPs via X-ray diffraction (XRD) (Figure S2). Matching our XRD pattern to Bruker's DIFFRAC.EVA structural database, we identified a primary phase of [Co(H₂O)₆](H₂PO₂)₂ (COD code: 2012913), along with smaller amounts of NH₄[CoPO₄(H₂O)] (COD code: 2008122), and LiC₂H₃O₂ (COD code: 7206368). LCP-NP XRD results were in agreement with the XPS analysis and indicate that the LCP-NPs contain multiple chemically distinct phases. This result is similar to prior studies of LiCoPO₄ synthesis, which have frequently reported multiple chemical and physical phases present, (Jaegermann 2010) due to the complex protonation chemistry of phosphate anions and the possibility of forming pyrophosphate and related phosphate species. (Han et al. 2006) We refer to the collective lithiated cobalt phosphate phases as "LCP" while recognizing that the material is not a single stoichiometric compound. In contrast, LCO-NPs could be referenced to the R-3m space group, consistent with that seen in the class of lithium intercalation based metal oxide materials and well-defined LiCoO₂ stoichiometry.(Hang et al. 2016)

Impact of LCO- and LCP-NP exposure on gill epithelial cell viability

To understand the possible implications of lithiated metal oxide and phosphate NPs released into the aquatic environment, we first determined the impact of NP exposure on the viability of Oncorhynchus mykiss (rainbow trout) gill epithelial cells. Nanoparticles released in the environment can encounter a myriad of different conditions, even across short spatial and temporal scales, which could impact their transformations. Since no prior studies focusing on the toxicity of LCO- or LCP- NPs in the gill epithelial cells have been conducted before, we chose to conduct exposures in the growth medium, which is required for the normal growth and health of the cells. By eliminating additional stress factors beyond the NPs themselves, it was possible to identify levels of NP toxicity and begin to decipher underlying mechanisms.

Cell viability was determined after a 3 h exposure to 1-100 μ g/mL LCO- and LCP-NPs using the MTS cell proliferation assay, and viability was normalized to unexposed control cells. For cells exposed to LCO-NPs, the lowest concentration observed to have a significant negative effect on cell viability was 10 μ g/mL (p < 0.01), which reduced viability to 93.9 \pm 2.0% (**Figure 2**). We observed a dose response for the concentration range from 10-100 μ g/mL, with viability decreasing to 78.3 \pm 2.1% at 50 μ g/mL and 69.3 \pm 2.3% at 100 μ g/mL. Interestingly, there was no reduction in viability of cells exposed to 1-100 μ g/mL LCP-NPs for 3 h. The effect of longer exposures (24 h) of 100 μ g/mL LCP- and LCO-NPs was also investigated. This exposure duration resulted in a reduction in cell viability for the LCP-NPs (90.5 \pm 1.6%), and a similar reduction in viability was observed for the LCO-NPs (70.7 \pm 1.2%) as compared to the 3 h exposure. Flow cytometry analysis of live and dead cell populations revealed similar trends: LCP-NPs minimally impacted cell viability while LCO-NPs reduced cell viability to 65.0 \pm 1.2% and 50.7 \pm 4.1% following a 24 h exposure to 50 and 100 μ g/mL nanoparticle concentrations, respectively (**Figure S3, Table S2**).

Nanoparticle internalization, dissolution, and toxicity of released metal ions

To investigate whether the observed toxic effects were primarily due to the release and toxicity of dissolved Co we first quantified the dissolution of both Li and Co from 100 μg/mL LCO- and LCP-NPs in Leibovitz's L-15 growth medium supplemented with 10% FBS (media), and in pH 4.5 artificial lysosomal fluid (ALF) for 0-48 h using ICP-MS. We observed a rapid release of Li⁺ from both NPs in media and ALF, and the acidic ALF had a minimal effect on increasing the concentration of dissolved Li (**Figure 3A**). The rapid release of Li⁺ has been previously observed for stoichiometric NMC NPs,(Hang et al. 2016) and it is most likely attributable to the favorable exchange with H⁺ from solution.(Huang et al. 2017) Concentrations of Li⁺ in the solutions ranged

from 760-870 μ M for LCO-NPs and 140-160 μ M for LCP-NPs at the end of the 48 h dissolution experiment. The acidic ALF solution had a much more pronounced effect on the release of Co ions (**Figure 3B**). After 48 h the concentration of Co²⁺ in solution was 50 μ M for LCO-NPs in media, but 480 μ M for the same particles in ALF. Similarly, after 48 h the concentration of Co²⁺ in solution was 180 μ M for LCP-NPs in media, and 350 μ M in ALF.

To test whether the observed reductions in cell viability (**Figure 2**) could be attributed to metal ion dissolution, we exposed the cells to Co^{2+} alone or Li^{+} and Co^{2+} in combination. Over a 24 h period, exposure to Co^{2+} alone with concentrations as high as 180 μ M or a combination of Co^{2+} and Li^{+} with concentrations as high as 480 μ M Co^{2+} and 870 μ M Li^{+} resulted in no reduction in cell viability (**Figure 4**).

To determine whether the cells can internalize the NPs used in this study we exposed cells to 10 μg/mL LCO- and LCP-NPs for 24 h, thin-sectioned the cell monolayers, and imaged the sections *via* transmission electron microscopy (TEM). Both LCO- and LCP-NPs were observed within membrane bound organelles (**Figure 5**), indicating that the trout gill epithelial cells do internalize both types of NPs. The TEM images also revealed certain cellular effects that were unique to LCO-NP exposure. First, the majority of the cells exposed to LCO-NPs showed extensive vacuole formation (**Figure 5A**, **Figure S4**). Additionally, internalized LCO-NPs were sometimes observed within multilamellar bodies (**Figure 5A**, **Figure S5**), which we did not observe for internalized LCP-NPs.

Impact of LCO- and LCP-NPs on intracellular reactive oxygen species (ROS) levels

Here we tested whether the exposure to lithiated metal oxide and phosphate NPs used in this study might alter intracellular levels of ROS. Following a 3 h exposure to $100 \mu g/mL$ LCO- and LCP-NPs the cells were incubated with CM-H₂DCFDA a general ROS fluorescent indicator. Fluorescence from the ROS indicator was minimal after exposure to LCP-NPs, but exposure to LCO-NPs resulted in high levels of intracellular ROS as indicated by the observed green fluorescence (**Figure 6**).

To gain a more quantitative analysis of ROS generation, we analyzed exposed cells by flow cytometry. Cells were exposed to 0, 50, and 100 μ g/mL LCO or LCP-NPs, as well as 100 and 1000 μ M Co²⁺ (from CoCl₂), for 3 and 24 h. Cells were then loaded with CM-H₂DCFDA and

fluorescence intensity for 10,000 cells per treatment groups was measured by flow cytomtery (**Figure S6**). Median values for each treatment group were normalized to the 0 μ g/mL NP treatment and are summarized in **Table 1**. Over both time periods there was minimal effect from Co²⁺ exposure alone, even at the 1000 μ M Co²⁺ concentration. At the 3 h time period, exposure to LCP-NPs resulted in a relatively small 2- and 2.5-fold increase in ROS indicator fluorescence (for 50 and 100 μ g/mL, respectively), but no increase was observed at the 24 h time period. Such transient increase in ROS has been observed before.(Xie et al. 2012) In agreement with the confocal imaging experiments (**Figure 6**), exposure to LCO-NPs resulted in a dramatic increase in intracellular ROS. Exposure to 50 and 100 μ g/mL LCO-NPs increased the fluorescence intensity 14- and 24-fold at the 3 h time point, respectively, and 5- and 6.5 fold at the 24 h time point, respectively.

Single cell p53 gene expression

As an initial step in investigating both the potential sub-toxic effects of LCO- and LCP-NPs and the anticipated variation across the gill epithelial cell population, we quantified p53 gene expression using single molecule fluorescence in situ hybridization (smFISH) at the single cell level. The expression of p53 is often monitored as an indicator of cell stress due to its function in DNA repair, cell cycle checkpoints, and initiation of apoptosis. (Liu & Kulesz-Martin 2001; Bartek & Lukas 2001; Ahamed et al. 2008) Cells were exposed to 1 and 100 μg/mL LCO- and LCP-NPs for 24 h prior to quantifying gene expression by smFISH. For both NPs investigated the 1 µg/mL concentration did not reduce cell viability (Figure 2). p53 mRNA copy number was quantified in 50-70 cells for each treatment condition. In unexposed control cells only 2% of the cells expressed more than 150 copies of p53 mRNA per cell (Figure 7, lower panel). We observed a large increase in p53 transcript copies per cell in cells exposed to 100 µg/mL of both LCO-NPs (83% > 150 copies, 34% > 300 copies) and LCP-NPs (62% > 150 copies, 13% > 300 copies). Interestingly, a clear increase in the number of p53 mRNA copies per cell was also observed at the sub-toxic 1 μg/mL NP exposure, with 52% and 57% of cells expressing more than 150 copies per cell in response to LCO or LCP-NPs, respectively. Exposure to 1 µg/mL LCO-NPs did appear to have a greater effect as 22% of the cells expressed more than 300 copies per cell, whereas only 5% of cells exposed to 1 µg/mL LCP-NPs showed such high level of expression. The distribution of p53 mRNA copy number per cell was relatively narrow in control cells, with an average of 69 ± 39

copies per cell. However, a large range in copy number per cell was observed in cells exposed to LCO- and LCP-NPs at 1 μ g/mL (average of 191 \pm 126 and 162 \pm 81 copy number per cell, respectively) and at 100 μ g/mL (average of 266 \pm 123 and 206 \pm 121 copy number per cell, respectively) (**Figure 7**).

DISCUSSION AND CONCLUSION

Viability assays indicated toxicity at a much lower concentration for the LCO-NPs as compared to the LCP-NPs. While we do acknowledge that there are caveats in comparing viability in response to NPs with varying composition and morphology, we would expect a greater load of LCP-NPs to reach the cells due to their larger size (increased sedimentation).(Hinderliter et al. 2010) However, the observed toxicity of LCO-NPs occurs at least at an order of magnitude lower mass concentration. These results point to a significant toxicity of the LCO-NPs. Previous studies with Shewanella oneidensis showed that NMC-NPs are not internalized by the Gram-negative bacteria, and that the primary driver of toxicity of these NPs is their dissolution and release of metal ions, specifically Ni²⁺ and Co²⁺. (Hang et al. 2016; Gunsolus et al. 2017) Given these results, we initially hypothesized that differential dissolution of LCO- and LCP-NPs, and the release of Co²⁺ ions, might be underlying the observed differences in their toxicity to the trout gill epithelial cells. Utilizing both bright-field microscopy and scanning electron microscopy we observed that the LCP-NPs were rapidly and completely dissolved (< 15 min; no visible NPs; Figure S7) after suspension in ALF, which explains the stable concentrations of Li⁺ and Co²⁺ released from LCP-NPs suspended in ALF over the 48 h period we investigated (Figure 3). Based on these trends, the acidic environments potentially encountered by internalized LCO- and LCP-NPs would be expected to enhance their dissolution and result in increased intracellular Co2+ and Li+ concentrations. Further, in the case of the LCP-NPs, rapid and complete dissolution is expected in acidic organelles.

In light of the NP dissolution results, our original hypothesis that Co^{2+} may be responsible for the observed reduction in the gill epithelial cell viability seemed less plausible, especially at the 3 h time point, as the release of Co ions from the less toxic LCP-NPs was greater than the release from the more toxic LCO-NPs in both media and ALF. Previous studies have shown that Co^{2+} toxicity can be induced at concentrations as low as ~2 μ M in bacteria(Hang et al. 2016) and ~40 μ M in

eukaryotic cells.(Huk et al. 2004; Papis et al. 2009) The gill epithelial cells have been shown to be more tolerant to Co²⁺ exposure, with concentrations as high as 51 μM showing no toxicity with exposure periods as long as three days.(Kühnel et al. 2009) Our results suggest that the trout gill epithelial cells are tolerant to Co²⁺ and Li⁺ exposure up to 480 μM Co²⁺ and 870 μM Li⁺ (**Figure** 4), and that the reduction in cell viability observed following exposure to LCO-NPs is nanoparticle specific and not due to metal ions released from the NPs.

NP internalization by eukaryotic cells can occur by a variety of pathways, (Gratton et al. 2008; Orr et al. 2007; Orr et al. 2009; Orr et al. 2011) including internalization via early endosomes that merge with acidic compartments, such as late endosomes and lysosomes. The acidic environment in these organelles can impact NP properties (Szymanski et al. 2015) and may enhance dissolution and increase the focal release of metal ions. (Muller et al. 2010; Mihai et al. 2015) While the internalization of the NPs used in this study by eukaryotic cells has not been previously investigated, the internalization of similarly-sized Co₃O₄-NPs aggregates by ECV-304 and HepG2 cells has been observed. (Papis et al. 2009) Based on the size of the NP aggregates we expected the gill epithelial cells to internalize both LCO- and LCP-NPs as tungsten carbide NP agglomerates as large as 1 µm in diameter have been observed to be internalized by these cells. (Kühnel et al. 2009) Our TEM results show that the trout gill cells are able to internalize both LCP- and LCO-NPs (Figure 5). Based on the NP aggregate size and the size of the observed organelles, it is possible that some of the observed organelles are acidic late endosome or lysosomes where LCP-NPs might be largely dissolved, as expected from the dissolution and EM studies in ALF described above (Figure 3).

Beyond demonstrating LCP- and LCO-NP internalization, the TEM images highlighted the extensive formation of vacuoles within some cells that internalized LCO-NPs (**Figure 5A**, **Figure S4**) and multilamellar bodies surrounding some LCO-NPs (**Figure 5A**, **Figure S5**). These were not observed in those cells exposed to LCP-NPs. An increase in the formation of multilamellar bodies has previously been reported in A549 human pneumocyte cells after exposure to multi-walled carbon nanotubes(Simon-Deckers et al. 2008) and SiO₂ NPs,(Shapero et al. 2011) and amine-modified polystyrene NPs have been observed within multilamellar bodies in 1321N1 human brain astrocytoma cells.(Bexiga et al. 2011) However, the physiological significance of multilamellar body formation upon exposure to NPs, or NP localization within multilamellar

bodies, was not discussed. Multilamellar bodies are found in specialized cells and are generally associated with the secretion of lipids or lipoproteins, such as the secretion of surfactants by type II alveolar epithelial cells. Under pathological conditions, however, multilamellar bodies may be found in other cell types,(Lajoie et al. 2005) as in the case of the brain astrocytoma cells exposed to polystyrene NPs(Bexiga et al. 2011) and in our study of trout gill epithelial cells exposed to LCO-NPs. The presence of autophagosomes has been implicated in contributing to the formation of multilamellar bodies,(Hariri et al. 2000; Lajoie et al. 2005) and might be related to some of the observed vacuoles in cells exposure to LCO-NPs. Several other studies have shown that NP exposure can lead to autophagosome accumulation.(Li et al. 2010; Ma et al. 2011; Bexiga et al. 2011)

A wealth of studies have implicated NP exposure with increasing intracellular reactive oxygen species (ROS) levels in eukaryotic cells. Several studies have demonstrated that exposure of cobalt-containing NPs can increase intracellular ROS, including cobalt-chromium(Behl et al. 2013) and cobalt oxide NPs.(Alinovi et al. 2015; Chattopadhyay et al. 2015; Limbach et al. 2007; Papis et al. 2009) Previous research has also shown that heavy metal ions (copper)(Bopp et al. 2008) and silver NPs(George et al. 2012) have the ability to increase intracellular levels of ROS in trout gill epithelial cells. We observed minimal ROS production in cells exposed to LCP-NPs, while those cells exposed to LCO-NPs showed extensive ROS production (Figure 6, Figure S6, **Table 1**). These results correlate with the cell viability data (**Figure 2**), which showed a significant reduction in cell viability after a 3 h exposure to 100 µg/mL LCO-NPs, whereas exposure to 100 µg/mL LCP-NPs did not reduce the viability of the cells. Earlier we described the extensive vacuole formation frequently observed in TEM images of cells exposed to LCO-NPs (Figure 5A, Figure S4), which could potentially be related to autophagosomes. There is an established link between NP-induced ROS generation and the formation of autophagosomes across a wide variety of cells and NPs.(Imran et al. 2012; Lee et al. 2014; Kenzaoui et al. 2012; Yu et al. 2013; Li et al. 2010) Our results may point to another example of the association between ROS and autophagosome accumulation as LCO-NP exposure greatly increased intracellular ROS levels (Figure 6), as well as vacuole formation (Figure 5a, Figure S4).

This dissimilarity in intracellular ROS production, coupled with cell viability results (**Figure 2**), highlight the stark difference in the effect of LCO-NP exposure as compared to LCP-NP exposure.

In the trout gill epithelial cells, exposure to and internalization of LCP-NPs appears to exert minimal negative impact. NPs may alter intracellular ROS levels *via* their direct generation at the NP surface or by disrupting cellular pathways that generate and control ROS.(Manke et al. 2013) While we did indicate that the synthesized LCP-NPs are not phase pure LiCoPO₄ based on our XPS and XRD characterization, the observed differences in oxidative stress could, in part, be due to the differences in oxidation state of Co in LCO- vs. LCP-NPs. In the LCO-NPs (LiCoO₂), Co is formally in the 3+ oxidation state, while in the LCP-NPs, Co is formally in the 2+ oxidation state in both Co-containing crystal phases identified by XRD ([Co(H₂O)₆](H₂PO₂)₂ and NH₄[CoPO₄(H₂O)]). In water, Co is stable in the 2+ oxidation state. Therefore, Co³⁺ in LCO-NPs would have to be reduced to Co²⁺ prior to dissolution. This process could result in the oxidation of water and the formation of ROS.(Zhang et al. 2014; Gunsolus et al. 2017) Future studies will elucidate the specific mechanisms behind ROS generation as ROS may be produced by the NPs themselves (possibly as described above), due to NP-induced interruption of cellular pathways, or a combination of both processes.

Data do not exist on the predicted environmental concentrations of lithiated metal oxide and phosphate NPs likely to be encountered in the environment. For those metal oxide NPs currently in extensive use across a variety of applications, namely TiO₂ and ZnO, recent modeling estimates predict concentrations in the range of 0.001-0.01 mg kg⁻¹ in surface waters in the year 2020.(Sun et al. 2016) The vast majority of research on the toxicity of engineered NPs employ viability assays that observe negative biological effects at exposure concentrations well above this range. Reported studies utilizing the trout gill cell line employed here include: minimum concentration effects on cell viability for tungsten carbide and tungsten carbide cobalt NPs at 8-30 µg/mL₂(Kühnel et al. 2009) EC₅₀ values $> 100 \mu g/mL$ for silica NPs,(Vo et al. 2014) and EC₅₀ values $> 1 \mu g/mL$ for silver NPs.(Yue et al. 2015) While these assays are helpful as an initial screening of the potential implications of NPs released into the aquatic environment, concentrations of NPs well below these reported concentrations may induce adverse effects that can alter or impair cellular function with no cell death. Investigating changes in gene expression, (Qiu et al. 2015; Hauck et al. 2008; Tilton et al. 2014) protein expression, (Jiang et al. 2008; Tilton et al. 2014) epigenetic modifications, (Choi et al. 2008; Gong et al. 2010) metabolomics, (Bo et al. 2014; Feng et al. 2013) and lipidomics (Yu et al. 2007) are possible means to assess adverse effects of NP exposure. Such studies are often

conducted at the cell population level, but studies have shown that the NP load experienced by cells exposed *in vitro* can vary several orders of magnitude, (Mitchell et al. 2016) and the response of cells exposed to the same concentration of NPs can vary dramatically based on factors such as NP load and cell cycle. (Kim et al. 2012; Mitchell et al. 2016)

We approached the difficulties outlined above in investigating NP concentrations that approach environmental relevance as well as investigating NP impacts at the single cell level, as opposed to the typical population-based approaches, by monitoring the expression of p53 in individual trout gill cells (**Figure 7**). The averaged values show no significant differences between control cells and cells exposed to LCP-NPs at both 1 and 100 µg/mL, nor between responses to LCO- and LCP-NPs, reiterating the importance of single cell analysis to identify subtle difference in cellular responses, especially at low sub-toxic NP concentrations. These results indicate that both LCO- and LCP-NPs impact the cells at concentrations that appear to have no effect by typical viability assays and begin to approach predicted environmental NP concentration values. These results also show that LCP-NPs, which have no impact on cell viability even at high concentrations, do increase the expression of genes involved in cellular response to stress.

Through these results, we have demonstrated that LCO-NPs have a greater negative impact on rainbow trout gill epithelial cells as compared to LCP-NPs. We observed both LCO- and LCP-NPs internalized by the gill epithelial cells and encased within membrane-bound organelles, likely to be endosomes or lysosomes, as well as multilamellar bodies in the case of LCO-NPs. Exposure to NP-free Li and Co ions at concentrations released from the NPs in growth medium and acidic artificial lysosomal fluid (as high as 480 µM Co²+ and 870 µM Li+) did not reduce cell viability. Further, the rapid and complete dissolution of LCP-NPs in artificial lysosomal fluid, together with their observed internalization into membrane-bound organelles and their minimal adverse effects on these cells, indicates that the dissolved ions are unlikely to underlie the toxicity of lithium and cobalt containing NPs within these cells. Thus, these observations point to the intact LCO-NP as the driver of its toxicity. The reduction in cell viability upon exposure to LCO-NPs was correlated with a large increase in intracellular ROS levels. Whether the primary driver of the large increase in ROS levels observed upon exposure to LCO-NPs is ROS generation at the NP surface (most likely as a result of Co reduction from +3 to +2) or by LCO-NPs interfering with cellular pathways controlling ROS generation and sequestration is unclear. Through TEM images we also observed

that LCO-NP exposure resulted in extensive intracellular vacuole formation (likely to be related to autophagosomes). To gain insight to molecular processes underlying these responses we quantified p53 gene expression in individual cells using single molecule FISH, which enabled the detection of subtle changes in cellular response to NP exposures at sub-toxic concentrations. We observed an increase in p53 gene expression per cell upon exposure to LCP-NPs at concentrations two orders of magnitude lower than the lowest concentration that impaired cell viability. We also observed an increase in p53 gene expression per cell in response to LCO-NPs at a sub-toxic concentration where no impact on cell viability could be detected. These results indicate that both LCP- and LCO-NPs do impact the cells at such low concentrations, but the cells are able to manage or repair cellular damage and prevent cell death at these concentrations. The averaged p53 gene expression values, however, showed no significant differences between control cells and cells exposed to LCP-NPs at both low and high concentrations (1 and 100 µg/mL), reiterating the importance of single cell analysis to identify subtle differences in cellular responses, especially at sub-toxic NP concentrations that begin to approach predicted environmental concentrations. With a wealth of technological drivers continually increasing the market for batteries with improved properties, studies such as this are imperative for building a thorough understanding of the potential environmental implications of the production, use, and disposal of nanoscale battery materials. Through this research informed decisions can be made on the use of nanoscale battery materials that are guided equally by economics, performance, and environmental sustainability.

ACKNOWLEDGMENTS

This work was supported by the National Science Foundation Center for Sustainable Nanotechnology (CHE-1503408), funded as a Center for Chemical Innovation. A portion of the research was performed using the Environmental Molecular Sciences Laboratory (EMSL), a DOE Office of Science User Facility sponsored by the Office of Biological and Environmental Research and located at the Pacific Northwest National Laboratory (PNNL).

DISCLOSURE STATEMENT

The authors declare no potential conflicts of interest.

REFERENCES

- Ahamed, M. et al., 2008. DNA damage response to different surface chemistry of silver nanoparticles in mammalian cells. *Toxicology and Applied Pharmacology*, 233(3), pp.404–410. Available at: http://dx.doi.org/10.1016/j.taap.2008.09.015.
- Alinovi, R. et al., 2015. Oxidative and pro-inflammatory effects of cobalt and titanium oxide nanoparticles on aortic and venous endothelial cells. *Toxicology in Vitro*, 29(3), pp.426–437. Available at: http://dx.doi.org/10.1016/j.tiv.2014.12.007.
- Bartek, J. & Lukas, J., 2001. Pathways governing G1/S transition and their response to DNA damage. *FEBS Letters*, 490, pp.117–122.
- Behl, B. et al., 2013. Biological effects of cobalt-chromium nanoparticles and ions on dural fibroblasts and dural epithelial cells. *Biomaterials*, 34(14), pp.3547–3558. Available at: http://dx.doi.org/10.1016/j.biomaterials.2013.01.023.
- Bexiga, M.G. et al., 2011. Cationic nanoparticles induce caspase 3-, 7- and 9- mediated cytotoxicity in a human astrocytoma cell line. *Nanotoxicology*, 5(4), pp.557–567.
- Bo, Y. et al., 2014. Metabolomic analysis on the toxicological effects of TiO2 nanoparticles in mouse fibroblast cells: from the perspective of perturbations in amino acid metabolism. *Toxicology Mechanisms and Methods*, 24(7), pp.461–469. Available at: http://www.tandfonline.com/doi/full/10.3109/15376516.2014.939321.
- Bopp, S.K., Abicht, H.K. & Knauer, K., 2008. Copper-induced oxidative stress in rainbow trout gill cells. *Aquatic Toxicology*, 86, pp.197–204.
- Bozich, J. et al., 2017. Core chemistry influences the toxicity of multicomponent metal oxide nanomaterials, lithium nickel manganese cobalt oxide, and lithium cobalt oxide to Daphnia magna. *Environmental Toxicology and Chemistry*, pp.1–10.
- Bruce, P.G., Scrosati, B. & Tarascon, J.-M., 2008. Nanomaterials for Rechargeable Lithium Batteries. *Angewandte Chemie International Edition*, 47(16), pp.2930–2946. Available at: http://doi.wiley.com/10.1002/anie.200702505.
- Chattopadhyay, S. et al., 2015. Toxicity of cobalt oxide nanoparticles to normal cells; an in vitro and in vivo study. *Chemico-Biological Interactions*, 226, pp.58–71. Available at: http://dx.doi.org/10.1016/j.cbi.2014.11.016.
- Choi, A.O. et al., 2008. Quantum dot-induced epigenetic and genotoxic changes in human breast cancer cells. *Journal of Molecular Medicine*, 86(3), pp.291–302.
- Cohen, J. et al., 2013. Interactions of engineered nanomaterials in physiological media and implications for in vitro dosimetry. *Nanotoxicology*, 7(4), pp.417–431.
- Dogangun, M. et al., 2015. Alteration of Membrane Compositional Asymmetry by LiCoO2 Nanosheets. *ACS nano*, 9(9), pp.8755–8765.
- Dunn, J.B. et al., 2015. The significance of Li-ion batteries in electric vehicle life-cycle energy and emissions and recycling's role in its reduction. *Energy & Environmental Science*, 8,

- pp.158–168. Available at: http://dx.doi.org/10.1039/C4EE03029J.
- Exnar, I. & Drezen, T., 2012. Synthesis of Nanoparticles of Lithium Metal Phosphate Positive Material for Lithium Secondary Battery.
- Feng, J. et al., 2013. Metabolic responses of HeLa cells to silica nanoparticles by NMR-based metabolomic analyses. *Metabolomics*, 9(4), pp.874–886.
- George, S. et al., 2012. Surface Defects on Plate-Shaped Silver Nanoparticles Contribute to Its Hazard Potential in a Fish Gill Cell Line and Zebra fish Embryos. *ACS Nano*, 6(5), pp.3745–3759.
- Gong, C. et al., 2010. SiO2 nanoparticles induce global genomic hypomethylation in HaCaT cells. *Biochemical and Biophysical Research Communications*, 397(3), pp.397–400. Available at: http://dx.doi.org/10.1016/j.bbrc.2010.05.076.
- Goodenough, J.B. & Park, K., 2013. The Li-Ion Rechargeable Battery: A Perspective. *Journal of the American Chemical Society*, 135, pp.1167–1176.
- Gratton, S.E.A. et al., 2008. The effect of particle design on cellular internalization pathways. *Proceedings of the National Academy of Sciences*, 105(33), pp.11613–11618.
- Gunsolus, I.L. et al., 2017. Influence of nickel manganese cobalt oxide nanoparticle composition on toxicity toward Shewanella oneidensis MR-1: redesigning for reduced biological impact. *Environ. Sci.: Nano*, 4, pp.636–646. Available at: http://xlink.rsc.org/?DOI=C6EN00453A.
- Han, Z. et al., 2006. A new three-dimensional cobalt phosphate: Co5(OH2)4(HPO4)2(PO4)2. *Journal of Solid State Chemistry*, 179, pp.3209–3213.
- Hang, M.N. et al., 2016. Impact of Nanoscale Lithium Nickel Manganese Cobalt Oxide (NMC) on the Bacterium Shewanella oneidensis MR-1. *Chemistry of Materials*, 28, pp.1092–1100.
- Hariri, M. et al., 2000. Biogenesis of Multilamellar Bodies via Autophagy. *Molecular Biology of the Cell*, 11, pp.255–268.
- Hauck, T.S., Ghazani, A.A. & Chan, W.C.W., 2008. Assessing the effect of surface chemistry on gold nanorod uptake, toxicity, and gene expression in mammalian cells. *Small*, 4(1), pp.153–159.
- Hedberg, Y., Hedberg, J. & Wallinder, I.O., 2012. Particle Characteristics and Metal Release from Natural Rutile (TiO2) and Zircon Particles in Synthetic Body Fluids. *Journal of Biomaterials and Nanobiotechnology*, 3, pp.37–49.
- Hinderliter, P.M. et al., 2010. ISDD: A computational model of particle sedimentation, diffusion and target cell dosimetry for in vitro toxicity studies ISDD: A computational model of particle sedimentation, diffusion and target cell dosimetry for in vitro toxicity studies. *Particle and Fibre Toxicology*, 7(36), pp.1–20.
- Huang, X. et al., 2017. Ab Initio Atomistic Thermodynamics Study of the (001) Surface of LiCoO 2 in a Water Environment and Implications for Reactivity under Ambient Conditions. *The Journal of Physical Chemistry C*, 121, pp.5069–5080.
- Huk, O.L. et al., 2004. Induction of apoptosis and necrosis by metal ions in vitro. *The Journal of Arthroplasty*, 19(8), pp.84–87. Available at: http://linkinghub.elsevier.com/retrieve/pii/S0883540304005108.
- Imran, M. et al., 2012. Induction of ROS, mitochondrial damage and autophagy in lung epithelial

- cancer cells by iron oxide nanoparticles. *Biomaterials*, 33, pp.1477–1488.
- Jaegermann, M.S.B.L.D.W., 2010. Preparation of LiCoPO4 powders and films via sol–gel. *Journal of Sol-Gel Science and Technology*, 56, pp.320–326.
- Jiang, W. et al., 2008. Nanoparticle-mediated cellular response is size-dependent. *Nature nanotechnology*, 3(3), pp.145–150.
- Kang, D.H.P., Chen, M. & Ogunseitan, O.A., 2013. Potential Environmental and Human Health Impacts of Rechargeable Lithium Batteries in Electronic Waste. *Environmental Science & Technology*, 47, pp.5495–5503.
- Kenzaoui, B.H. et al., 2012. Induction of oxidative stress, lysosome activation and autophagy by nanoparticles in human brain-derived endothelial cells. *Biochemical Journal*, 441, pp.813–821.
- Kim, J.A. et al., 2012. Role of cell cycle on the cellular uptake and dilution of nanoparticles in a cell population. *Nature Nanotechnology*, 7, pp.62–68.
- Kittler, S. et al., 2010. Toxicity of Silver Nanoparticles Increases during Storage Because of Slow Dissolution under Release of Silver Ions. *Chemistry of Materials*, 22, pp.4548–4554.
- Kühnel, D. et al., 2009. Agglomeration of tungsten carbide nanoparticles in exposure medium does not prevent uptake and toxicity toward a rainbow trout gill cell line. *Aquatic Toxicology*, 93(2–3), pp.91–99.
- Lajoie, P. et al., 2005. The lipid composition of autophagic vacuoles regulates expression of multilamellar bodies. *Journal of Cell Science*, 118, pp.1991–2003.
- Lee, J., Kim, T. & Park, B., 2007. Metal-phosphate coating on LiCoO2 cathodes with high cutoff voltages. *Materials Research Bulletin*, 42, pp.1201–1211.
- Lee, Y.-H. et al., 2014. Cytotoxicity, oxidative stress, apoptosis and the autophagic effects of silver nanoparticles in mouse embryonic fibroblasts. *Biomaterials*, 35, pp.4706–4715.
- Li, J.J. et al., 2010. Autophagy and oxidative stress associated with gold nanoparticles. *Biomaterials*, 31, pp.5996–6003.
- Limbach, L.K. et al., 2007. Exposure of engineered nanoparticles to human lung epithelial cells: Influence of chemical composition and catalytic activity on oxidative stress. *Environmental Science & Technology*, 41(11), pp.4158–4163.
- Liu, Y. & Kulesz-Martin, M., 2001. p53 protein at the hub of cellular DNA damage response pathways through sequence-specific and non-sequence-specific DNA binding. *Carcinogenesis*, 22(6), pp.851–860.
- Lu, Z. et al., 2014. Electrochemical tuning of layered lithium transition metal oxides for improvement of oxygen evolution reaction. *Nature Communications*, 5, pp.1–7.
- Ma, X. et al., 2011. Gold Nanoparticles Induce Autophagosome Accumulation through Size-Dependent Nanoparticle Uptake and Lysosome Impairment. *ACS Nano*, 5(11), pp.8629–8639.
- Manke, A., Wang, L. & Rojanasakul, Y., 2013. Mechanisms of Nanoparticle-Induced Oxidative Stress and Toxicity. *BioMed Research International*, pp.1–15.
- Mihai, C. et al., 2015. Intracellular accumulation dynamics and fate of zinc ions in alveolar

- epithelial cells exposed to airborne ZnO nanoparticles at the air liquid interface. *Nanotoxicology*, 9(1), pp.9–22.
- Mitchell, H.D. et al., 2016. Cells Respond to Distinct Nanoparticle Properties with Multiple Strategies as Revealed by Single-Cell RNA-Seq. *ACS Nano*, 10, pp.10173–10185.
- Muller, K.H. et al., 2010. pH-Dependent Toxicity of High Aspect Ratio ZnO Nanowires in Macrophages Due to Intracellular Dissolution. *ACS Nano*, 4(11), pp.6767–6779.
- Nitta, N. et al., 2015. Li-ion battery materials: present and future. *Materials Today*, 18(5), pp.252–264. Available at: http://dx.doi.org/10.1016/j.mattod.2014.10.040.
- Orr, G. et al., 2007. Submicrometer and Nanoscale Inorganic Particles Exploit the Actin Machinery To Be Propelled along Microvilli-like Structures into Alveolar Cells. *ACS Nano*, 1(5), pp.463–475.
- Orr, G. et al., 2009. Syndecan-1 mediates the coupling of positively charged submicrometer amorphous silica particles with actin filaments across the alveolar epithelial cell membrane. *Toxicology and Applied Pharmacology*, 236(2), pp.210–220. Available at: http://dx.doi.org/10.1016/j.taap.2009.01.022.
- Orr, G.A. et al., 2011. Cellular recognition and trafficking of amorphous silica nanoparticles by macrophage scavenger receptor A. *Nanotoxicology*, 5(3), pp.296–311.
- Papis, E. et al., 2009. Engineered cobalt oxide nanoparticles readily enter cells. *Toxicology Letters*, 189(3), pp.253–259.
- Poizot, P. et al., 2000. Nano-sized transition-metal oxides as negative-electrode materials for lithium-ion batteries. *Science*, 407, pp.496–499.
- Qian, D. et al., 2012. Electronic Spin Transition in Nanosize Stoichiometric Lithium Cobalt. Journal of the American Chemical Society, 134, pp.6096–6099.
- Qiu, T.A. et al., 2015. Gene expression as an indicator of the molecular response and toxicity in the bacterium Shewanella oneidensis and the water flea Daphnia magna exposed to functionalized gold nanoparticles. *Environ. Sci.: Nano*, 2(6), pp.615–629. Available at: http://xlink.rsc.org/?DOI=C5EN00037H.
- Raj, A. et al., 2008. Imaging individual mRNA molecules using multiple singly labeled probes. *Nature Methods*, 5(10), pp.877–879.
- Raj, A. & Tyagi, S., 2010. Chapter 17 Detection of Individual Endogenous RNA Transcripts In Situ Using Multiple Singly Labeled Probes. In *Methods in Enzymology Single Molecule Tools: Fluorescence Based Approaches, Part A.* pp. 365–386. Available at: http://www.sciencedirect.com/science/article/pii/S0076687910720048 [Accessed June 2, 2017].
- Shapero, K. et al., 2011. Time and space resolved uptake study of silica nanoparticles by human cells. *Molecular BioSystems*, 7, pp.371–378.
- Simon-Deckers, A. et al., 2008. In vitro investigation of oxide nanoparticle and carbon nanotube toxicity and intracellular accumulation in A549 human pneumocytes. *Toxicology*, 253, pp.137–146.
- Sun, T.Y. et al., 2016. Dynamic Probabilistic Modeling of Environmental Emissions of Engineered Nanomaterials. *Environmental Science and Technology*, 50(9), pp.4701–4711.

- Szymanski, C.J. et al., 2015. Shifts in oxidation states of cerium oxide nanoparticles detected inside intact hydrated cells and organelles. *Biomaterials*, 62, pp.147–154.
- Tilton, S.C. et al., 2014. Three human cell types respond to multi-walled carbon nanotubes and titanium dioxide nanobelts with cell-specific transcriptomic and proteomic expression patterns. *Nanotoxicology*, 8(5), pp.533–48. Available at: http://www.pubmedcentral.nih.gov/articlerender.fcgi?artid=4226242&tool=pmcentrez&ren dertype=abstract.
- Vo, N.T.K. et al., 2014. Cytotoxicity evaluation of silica nanoparticles using fish cell lines. *In Vitro Cellular and Developmental Biology Animal*, 50(5), pp.427–438.
- Wang, H. et al., 2007. Effect of LiFePO4 coating on electrochemical performance of LiCoO2 at high temperature. *Solid State Ionics*, 178, pp.131–136.
- Wang, H. et al., 1999. TEM Study of Electrochemical Cycling-Induced Damage and Disorder in LiCoO 2 Cathodes for Rechargeable Lithium Batteries. *Journal of The Electrochemical Society*, 146(2), pp.473–480.
- Wang, J. et al., 2017. Ultrathin LiCoO2 Nanosheets: An Efficient Water-Oxidation Catalyst. *Applied Materials and Interfaces*, 9, pp.7100–7107.
- Wu, T. et al., 2017. Identifying the Active Surfaces of Electrochemically Tuned LiCoO 2 for Oxygen Evolution Reaction. *Journal of the American Chemical Society*, 139, pp.6270–6276.
- Xia, T. et al., 2008. Comparison of the mechanism of toxicity of zinc oxide and cerium oxide nanoparticles based on dissolution and oxidative stress properties. *ACS nano*, 2(10), pp.2121–2134. Available at: http://doi.wiley.com/10.1002/cite.200950629.
- Xie, Y. et al., 2012. Aerosolized ZnO Nanoparticles Induce Toxicity in Alveolar type II Epithelial Cells at the Air-Liquid Interface. *Toxicological Sciences*, 125(2), pp.450–461.
- Yu, K.-N. et al., 2013. Zinc oxide nanoparticle induced autophagic cell death and mitochondrial damage via reactive oxygen species generation. *Toxicology in Vitro*, 27, pp.1187–1195.
- Yu, L.E. et al., 2007. Translocation and effects of gold nanoparticles after inhalation exposure in rats. *Nanotoxicology*, 1(3), pp.235–242. Available at: http://www.tandfonline.com/doi/full/10.1080/17435390701763108 [Accessed June 3, 2017].
- Yue, Y. et al., 2016. Silver nanoparticles inhibit fish gill cell proliferation in protein-free culture medium. *Nanotoxicology*, 10(8), pp.1075–1083.
- Yue, Y. et al., 2015. Toxicity of silver nanoparticles to a fish gill cell line: Role of medium composition. *Nanotoxicology*, 9(1), pp.54–63. Available at: http://www.tandfonline.com/doi/full/10.3109/17435390.2014.889236.
- Zaghib, K. et al., 2013. Review and analysis of nanostructured olivine-based lithium recheargeable batteries: Status and trends. *Journal of Power Sources*, 232, pp.357–369.
- Zaghib, K. et al., 2011. Safe and fast-charging Li-ion battery with long shelf life for power applications. *Journal of Power Sources*, 196, pp.3949–3954. Available at: http://dx.doi.org/10.1016/j.jpowsour.2010.11.093.
- Zhang, M., de Respinis, M. & Frei, H., 2014. Time-resolved observations of water oxidation intermediates on a cobalt oxide nanoparticle catalyst. *Nature Chemistry*, 6, pp.362–367. Available at: http://dx.doi.org/10.1038/nchem.1874.

FIGURE LEGENDS

Figure 1. Transmission electron micrographs of (A) LCO and (B) LCP-NPs. NPs were sonicated for 10 minutes in water and drop cast on a TEM grid prior to imaging.

Figure 2. Viability of trout gill epithelial cells after a 3 h exposure to 1-100 μ g/mL LCP- and LCO-NPs. * indicates statistically significant reduction in viability compared to unexposed control cells (p < 0.01). Bars represent mean values; error bars correspond to one standard deviation for six experimental replicates. Viability was determined by the MTS cell proliferation assay, and cell viability was normalized to unexposed control cells. LCP, lithiated cobalt hydroxyphosphate; LCO, lithium cobalt oxide.

Figure 3. The dissolution of (A) Li⁺ and (B) Co²⁺ from LCO- and LCP-NPs was determined by ICP-MS for nanoparticles suspended in both Leibovitz's L-15 media supplemented with 10% fetal bovine serum (Media) and artificial lysosomal fluid (ALF) for 0-48 hours. Error bars correspond to one standard deviation for three experimental replicates.

Figure 4. Viability of RTgill-W1 cells was determined after a 24 h exposure to the concentration of ions determined to dissolve from LCO- and LCP-NPs (Fig. 4) suspended in both Leibovitz's L-15 media supplemented with 10% fetal bovine serum (Media) and artificial lysosomal fluid (ALF) using the MTS cell proliferation assay. Bars represent mean values; error bars correspond to one standard deviation for six experimental replicates. Exposure concentrations: 55 μM Co²⁺, 180 μM Co²⁺, 55 μM Co²⁺ and 760 μM Li⁺, 180 μM Co²⁺ and 140 μM Li⁺, 480 μM Co²⁺ and 870 μM Li⁺, and 350 μM Co²⁺ and 160 μM Li⁺.

Figure 5. Transmission electron micrographs of gill cells exposed to LCO (A&B) and LCP (C&D) NPs reveal that both types of NPs are internalized by the cells and found within membrane-bound organelles.

Figure 6. Gill cells were stained with Hoechst (nuclei, blue) and CM-H₂DCFDA (ROS, green) to determine relative intracellular levels of reactive oxygen species (ROS) after a 3 h exposure to either 0 μg/mL (unexposed), 100 μg/mL LCP-NPs, or 100 μg/mL LCO-NPs. LCP, lithiated cobalt hydroxyphosphate; LCO, lithium cobalt oxide. Scale bar is 20 μm.

Figure 7. Single molecule FISH was used to quantify p53 mRNA copy number in individual trout gill epithelial cells (n = 50-70 individual cells) exposed to 0, 1, and 100 μ g/mL LCO- and LCP-NPs. Values provided for each treatment group is the average mRNA copy number \pm standard deviation. Examples of DIC and fluorescence images are shown on the right for each treatment group. Nuclei are shown in blue (DAPI) and red dots represent mRNA copies. Scale bars are 10 μ m.

	^0 μg/mL	^100 μg/mL	^100 μg/mL	100 μM	1000 μΜ	50 μg/mL	100 μg/mL	50 μg/mL	100 μg/mL
		LCO	LCP	Co^{2+}	Co^{2+}	LCP	LCP	LCO	LCO
3 h	0.3 ± 0.01	0.30	0.3	1.2 ± 0.4	1.3	1.9 ± 0.1	2.5 ± 0.2	14.3 ± 1.2	23.8 ± 5.5
24 h	0.2	N/A	N/A	1.0 ± 0.1	1.0	0.6 ± 0.01	0.8 ± 0.04	5.1 ± 0.1	6.5 ± 0.1

Table 1. Median fluorescence intensity values of 10,000 trout gill epithelial cells per treatment group acquired by flow cytometry. Cells were loaded with 0 or 10 μM CM-H₂DCFDA following exposure to 0, 50, and 100 μg/mL LCO- and LCP-NPs as well as 100 and 1000 μM Co²⁺ (from CoCl₂). Median fluorescence intensity was normalized to 0 μg/mL cells loaded with 10 μM CM-H₂DCFDA. Standard deviation is provided for exposures where N = 2-3. ^Indicates 0 μM CM-H₂DCFDA treatment (to determine background fluorescence). N/A indicates a condition that was not analyzed.

Figure 1

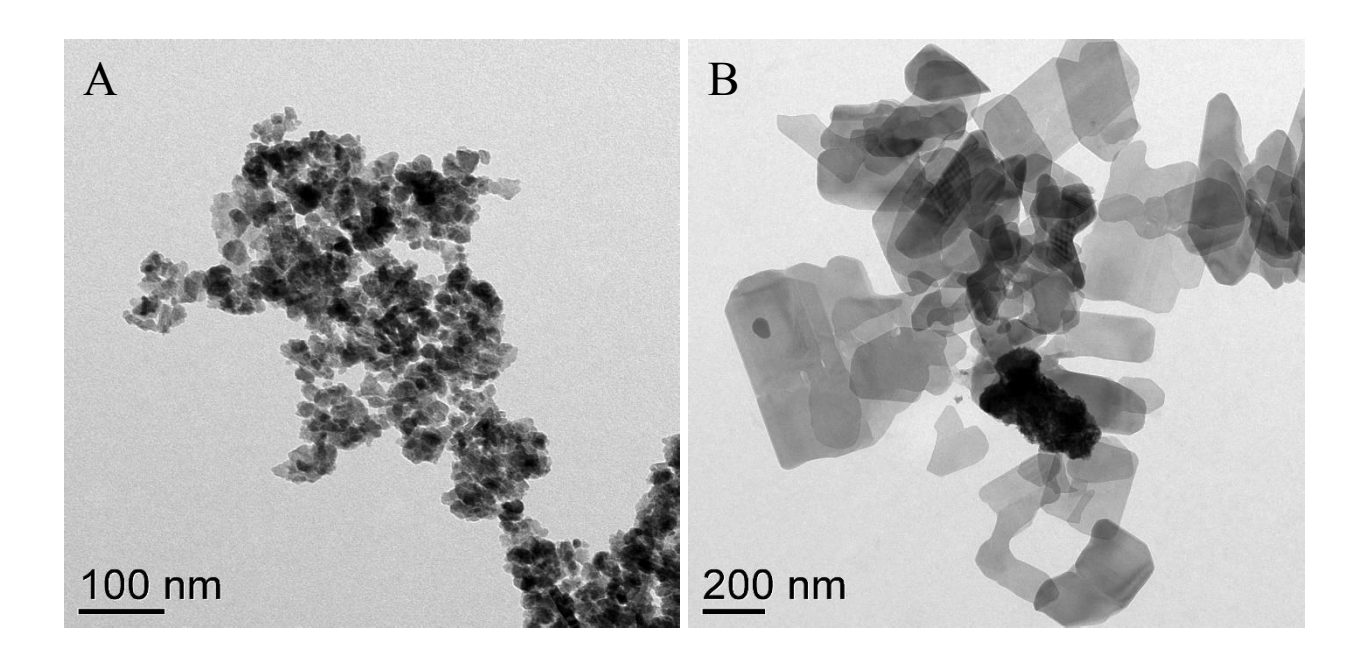


Figure 2

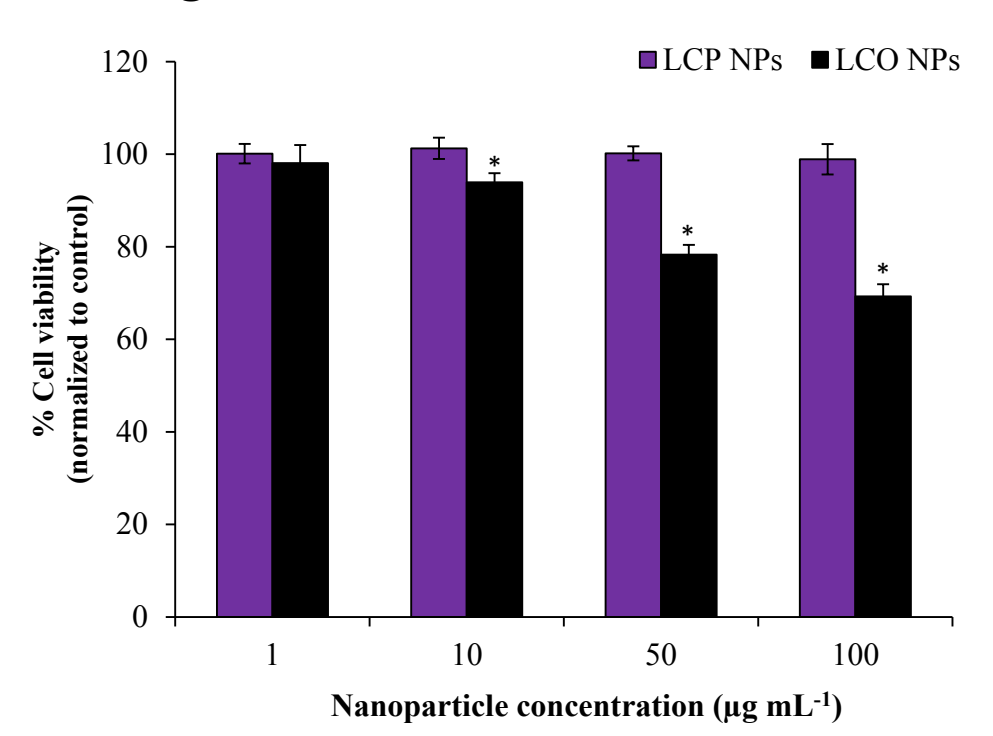
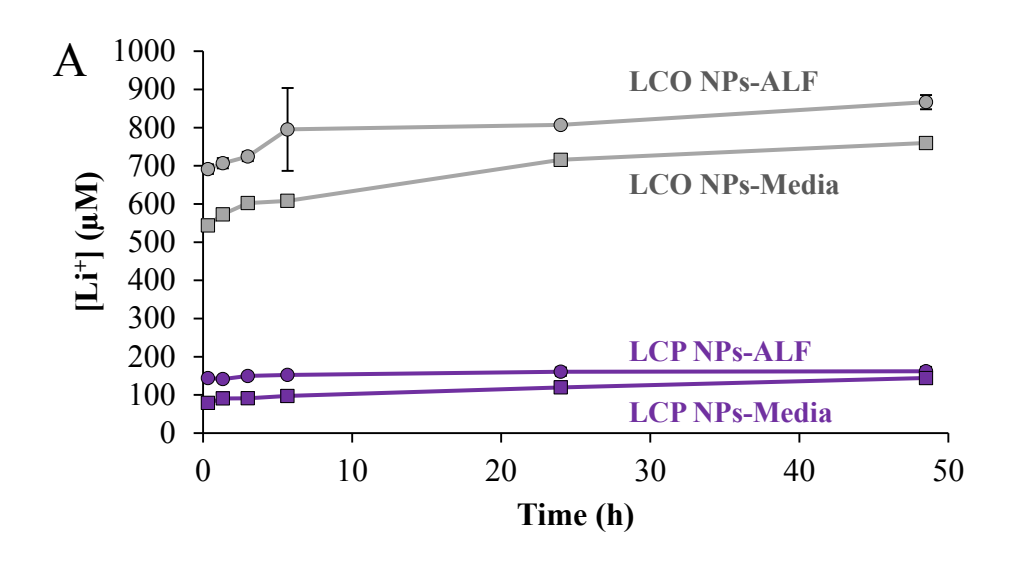


Figure 3



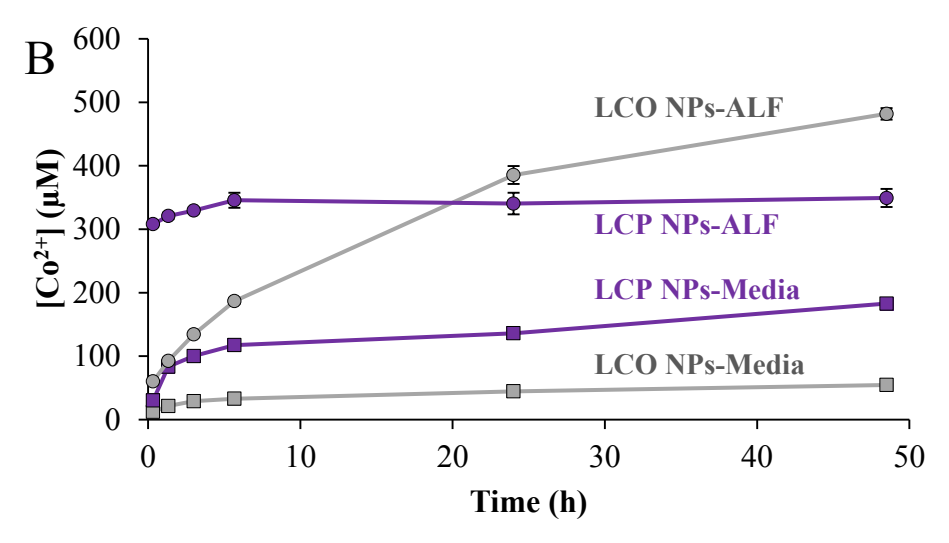


Figure 4

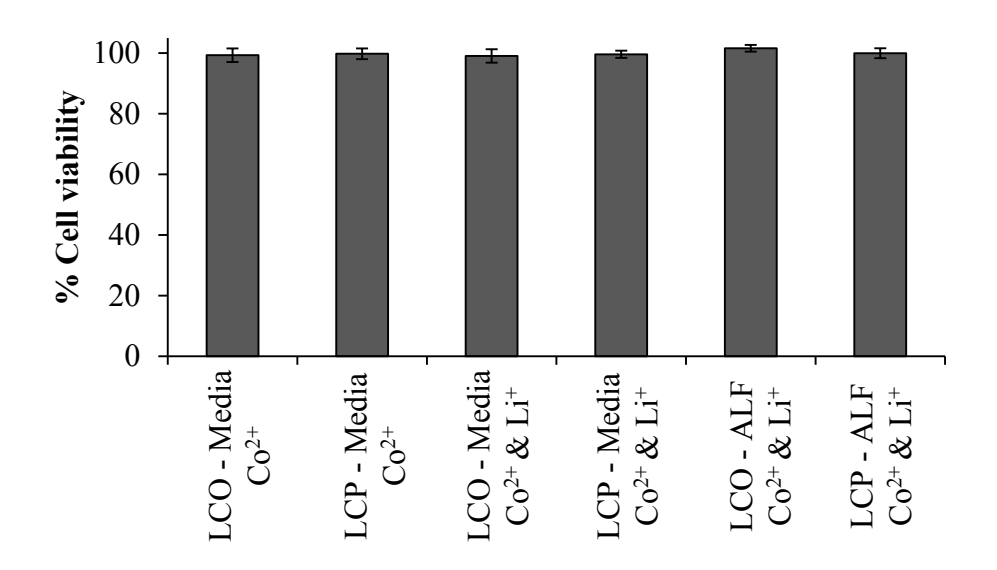


Figure 5

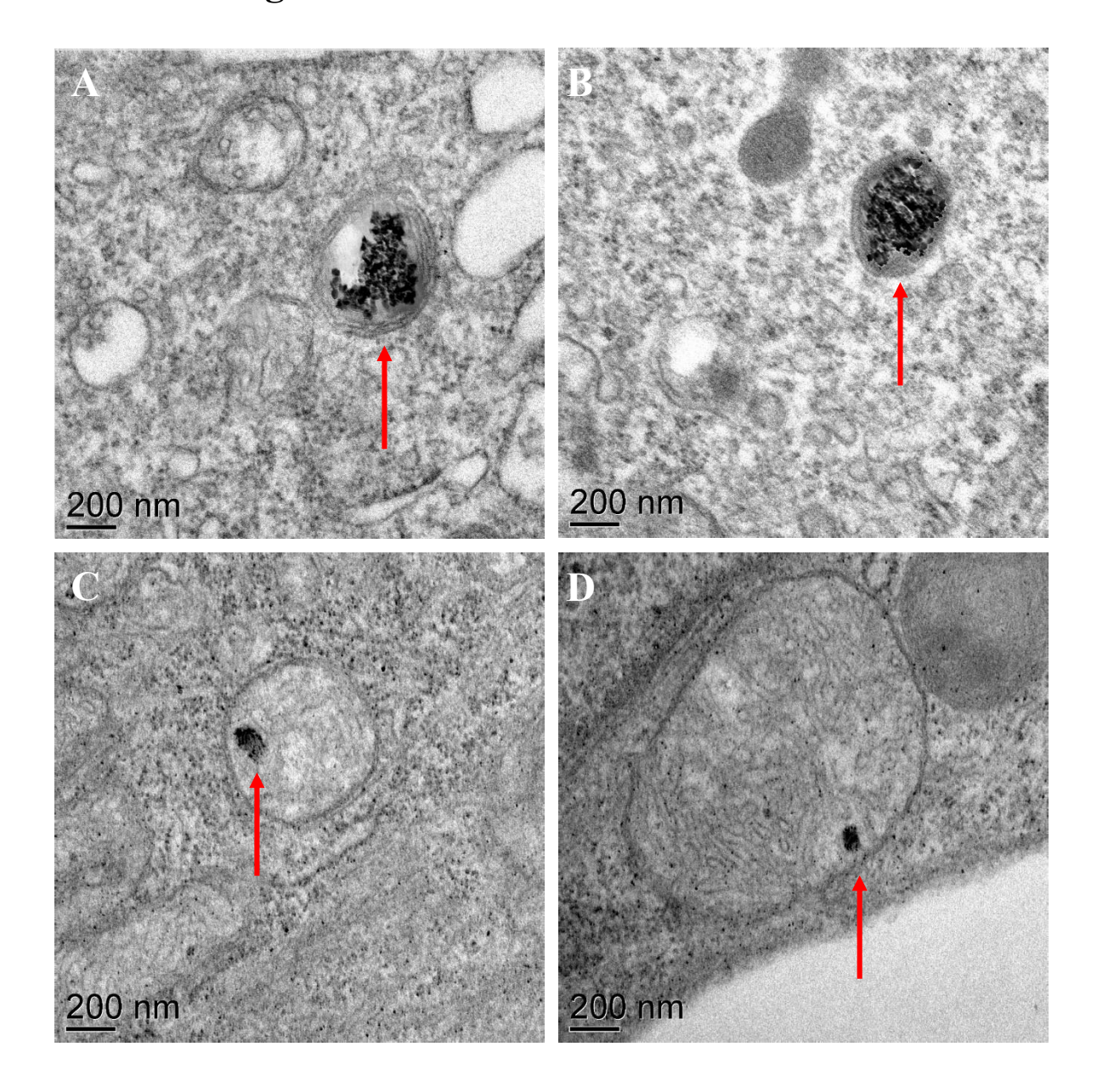
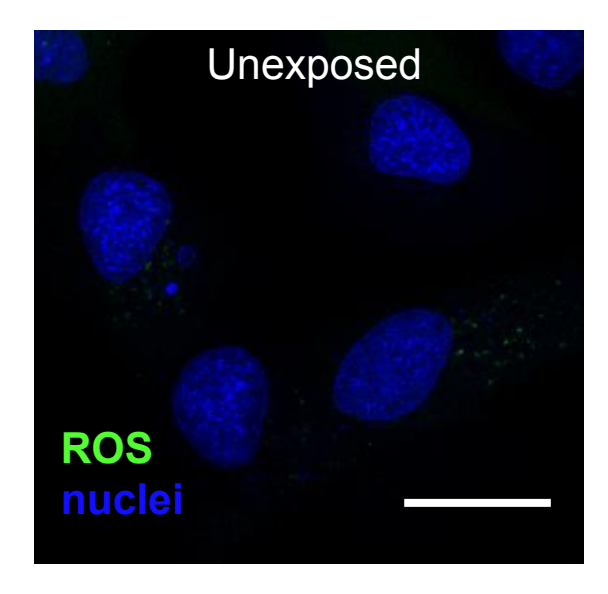
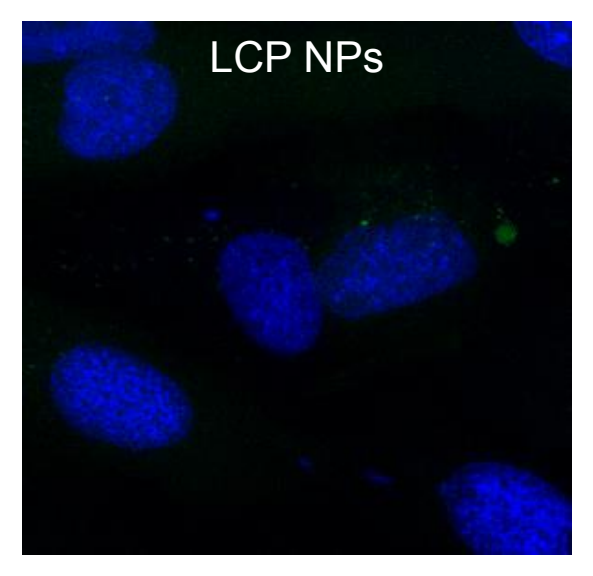


Figure 6





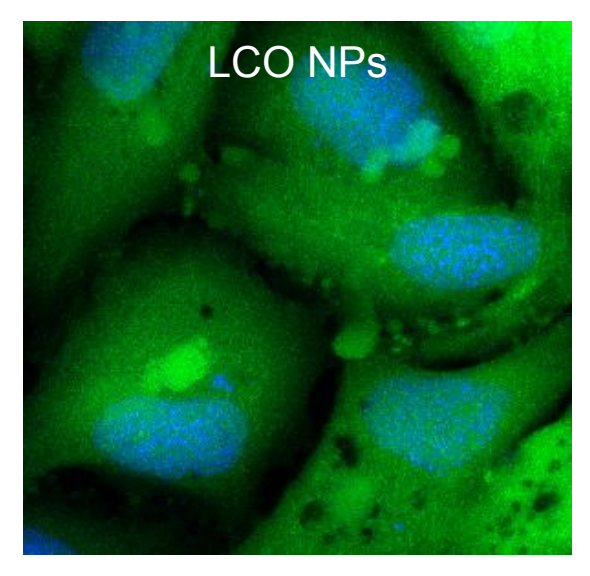


Figure 7

